13. Traverse Gravimeter Experiment

Manik Talwani,[a†] *George Thompson,*[b] *Brian Dent,*[b] *Hans-Gert Kahle,*[a] *and Sheldon Buck*[c]

The primary goal of the traverse gravimeter experiment (TGE) was to make relative gravity measurements at a number of sites in the Apollo 17 landing area and to use these measurements to obtain information about the geological substructure. A secondary goal was to obtain the value of the gravity at the landing site relative to an accurately known value on Earth. Both these goals were successfully achieved by the experiment. A gravity tie has been obtained between the Taurus-Littrow landing site and the Earth with an estimated accuracy of approximately 5 mgal. Relative gravity measurements that can be used to infer the substructure of the area have been obtained at stations visited during each period of extravehicular activity (EVA).

BASIC THEORY

Free-Air and Bouguer Anomalies

The basic theory for the interpretation of the traverse gravity measurements can be described with the help of the sketch in figure 13-1. As a simplifying approximation, two-dimensionality is assumed; the sketch is a hypothetical geological cross section. The gravity measurements are made at the lunar module (LM) landing site and at certain stations (stations 1, 2, 3, 4, 5, etc.). The gravity value at the LM site is subtracted from the values at the other stations, and, for this report, only the relative values at the stations will be considered.

The first step in the interpretation of the relative gravity values is to make the free-air correction for elevation; that is, to allow for the differences in the distances of these stations from the center of the Moon. If g_m denotes the gravity at the surface of the Moon, M the mass of the Moon, r the radius of the Moon, and k the universal constant of gravitation, then

$$g_m = \frac{kM}{r^2} \tag{13-1}$$

The free-air gradient then is

$$\frac{\partial g_m}{\partial r} = \frac{-2kM}{r^3} = \frac{-2g_m}{r} \tag{13-2}$$

and the free-air correction is $2g_m/r$, which yields a value of 0.19 mgal/m. The elevation in meters is measured from an arbitrary elevation datum (fig. 13-1). The free-air correction is added to the relative gravity values to obtain the free-air anomalies.

The next step in the interpretation of the free-air anomalies involves the Bouguer correction. The Bouguer correction allows for the gravity effect (i.e., the vertical component of the gravitational attraction) of the material above the elevation datum

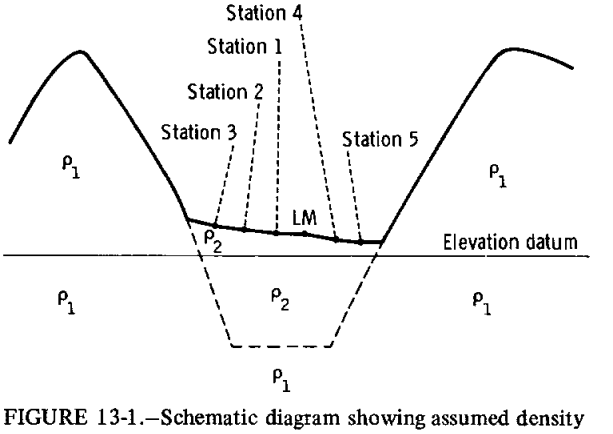

FIGURE 13-1.–Schematic diagram showing assumed density configurations for a hypothetical geological cross section.

[a]Lamont-Doherty Geological Observatory.
[b]Stanford University.
[c]Charles Draper Laboratory, Massachusetts Institute of Technology.
[†]Principal Investigator.

computed at the gravity stations. This correction involves a knowledge of the density of the material above the elevation datum. In the sketch in figure 13-1, densities of ρ_1 for the material comprising the massifs and ρ_2 for the material of the valley floor have been assumed. The fact that the actual situation can be much more complicated must be considered in the interpretation of the Bouguer anomalies.

In gravity interpretation, the Bouguer correction is usually applied in two steps. The first, the flat-plate Bouguer, assumes that the elevation is the same at all points as at the station where the correction is being applied. The second, the terrain correction, allows for the departure of the actual terrain from a plane at the height of the station. For the Taurus-Littrow landing site, the terrain corrections are large, and no particular advantage is gained by computing the flat-plate Bouguer corrections and the terrain corrections separately. By computing the gravity effect of all the material above the elevation datum with a single computation, the combined Bouguer correction is applied, and, by adding it to the free-air anomaly, the Bouguer anomaly is obtained. In these calculations of the Bouguer corrections, a flat Moon rather than a spherical Moon is used. The relative error at the different stations is negligible for the present calculations.

The final step is the interpretation of the Bouguer anomalies. The Bouguer anomalies have allowed for the elevation differences between the different stations and for the gravitational effect of the material above the elevation datum. Therefore, the Bouguer anomalies are interpreted in terms of, and provide information about, the density contrasts of rocks lying below the elevation datum. In the simplified model shown in figure 13-1, for instance, the density contrast $\rho_1 - \rho_2$ between the material comprising the massifs and the material lying below the valley floor gives rise to the Bouguer anomalies at the stations. The actual structural situations as well as the density variations are probably much more complicated than those shown in the sketch. The interpretation approach will be to work with simple models consistent with available geological information and to see how these models explain the gravity data. The final structural solution will be constrained by the gravity results, by considerations of geological plausibility, and by the results from the other geological and geophysical data.

Two-Dimensional Calculations

As a first approximation, two-dimensionality is assumed. The gravity effect of a body is obtained by approximating its cross section by an irregular polygon. The gravity effect of a body with a polygonal cross section has been given by Talwani et al. (ref. 13-1).

Three-Dimensional Calculations

For more careful analysis of the gravity data, it is essential both to compute the Bouguer anomalies and to interpret them without the assumption of two-dimensionality. The basic formula used in this calculation is the gravity effect of a vertical prism, which is given by Jung (ref. 13-2). For distant areas, prisms of large area can be chosen and an average elevation assumed for them. For closer areas, prisms of smaller area must be chosen. By actual trial and error, prisms of optimum area are chosen at various distances from the landing site for use in the calculations. Such a determination has been made. The three-dimensional calculations are not complete at the present time, and only the results of two-dimensional calculations will be discussed in this report.

EQUIPMENT

Sensor

The gravity sensor used in the TGE is a Bosch Arma D4E vibrating string accelerometer (VSA). The accelerometer is schematically shown in figure 13-2. Each of the two strings, when energized, generates continuous vibrations with its own frequency, the value of which depends on the value of g. The difference between the two frequencies can be obtained. The difference frequency between the two strings Δf_n when the sensor is in its normal vertical position can be written as

$$\Delta f_n = k_0 + k_1 g + k_2 g^2 + k_3 g^3 + \ldots \quad (13\text{-}3)$$

Terms of order higher than 3 can be neglected. Nominal values for k_0, k_1, et cetera, for the flight vibrating string accelerometers are $k_0 = 7$ Hz, $k_1 = 129$ Hz/g, $k_2 = -0.00034$ Hz/g^2, and $k_3 = 0.003$ Hz/g^3. A principal reason for the use of a double-stringed rather than a single-stringed instrument is the

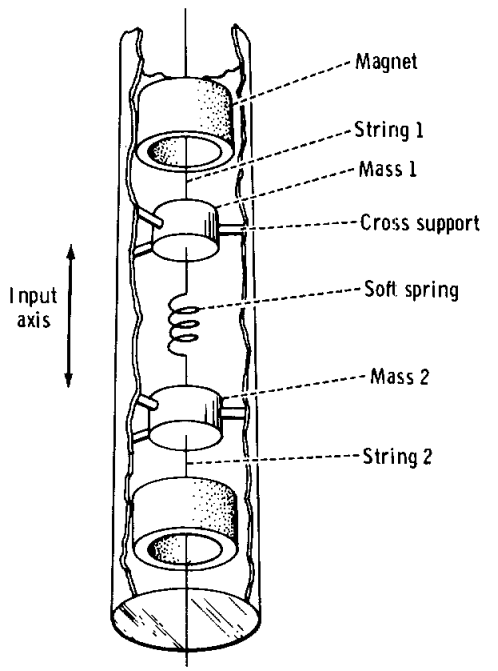

FIGURE 13-2.–Schematic view of double-stringed VSA.

reduction in the values of the higher order terms. Even-order terms of the type $k_2 g^2$ give rise to nonlinear rectification of inertial accelerations caused by vibrations; therefore, it is very important to keep the terms small.

The constants k_0, k_1, k_2, and k_3 are determined for the sensor before the mission. However, experience with sensors of this type had shown that k_0 is subject to drift as well as tares (sudden dc shifts). Any shift of k_0 would degrade the Earth-Moon gravity tie. (Shifts in k_1, k_2, etc., are much less important.) Also, if, at a station during a traverse, a large difference of gravity from the value at the LM site was indicated, it would be necessary to inquire whether this was a real variation in gravity or whether the value of k_0 had shifted. For this reason, provision was made to make independent determinations of k_0 when necessary. Such a determination is called a bias determination and is made by inverting the instrument. In the inverted case

$$\Delta f_i = -k_0 + k_1 g - k_2 g^2 + k_3 g^3 \qquad (13\text{-}4)$$

By assuming the values of k_1, k_2, and k_3, the values of k_0 and g can be determined from the values of Δf_n and Δf_i by combining equations (13-3) and (13-4).

Filtering and Phase Lock Loop

The electrically conducting VSA strings are placed in a permanent magnetic field (fig. 13-2). When a voltage is applied across the string, the resulting current causes motion of the string and induces a voltage across the string. The voltage is regenerated through a stable, high-gain amplifier and fed back to the string.

The output of each VSA string is a sine wave of a frequency between 9.25 and 9.75 kHz. The signal is fed to a phase lock loop module. The purposes of the phase lock loop module are to determine the difference frequency between the outputs of the two strings and to filter the effect of undesirable vibrations from the resultant signal.

Should any vibrations cause the input frequency from the VSA to exceed a previously specified limit, a phase lock loop alarm is generated. This alarm is indicated by the TGE display.

Measurement

Because the lunar value of g is approximately 163 000 mgal and a measurement to the precision of 0.1 mgal is desired, the difference frequency of the VSA must be measured to an accuracy of approximately 1×10^{-6}. Because the nominal values of the difference frequencies in the normal and inverted positions are approximately 28 and 14 Hz, respectively, a simple counting of the cycles obviously will take an impossibly long time. Instead, a gate is generated that is inversely proportional to the difference frequency. For the normal case, the gate consists of 1536 cycles of the difference frequency Δf_n (approximately 55 sec at this frequency); for the inverted case, the gate consists of 384 cycles of the difference frequency Δf_i (approximately 27 sec). The width of the gate is measured by counting the pulses from a precision 125-kHz clock by a counter. If D_n and D_i are the counts in the normal and inverted case

$$\Delta f_n = \frac{1536 \times 125 \times 10^3}{D_n} = \frac{1.92 \times 10^8}{D_n} \qquad (13\text{-}5)$$

$$\Delta f_i = \frac{384 \times 125 \times 10^3}{D_i} = \frac{4.8 \times 10^7}{D_i} \qquad (13\text{-}6)$$

If k_0, k_1, k_2, and k_3 are all known, equation (13-3) can be used to determine the value of g from Δf_n. If

k_0 is not assumed to be known, equations (13-3) and (13-4) together can be used to determine the value of g as well as k_0 from Δf_n and Δf_i.

Leveling

If the VSA axis is not vertical but is inclined at an angle θ to the vertical, $g \cos \theta$ is measured instead of θ. For a small θ, the error is $0.5g\theta^2$. The TGE is designed to keep θ less than 00°03′ of arc and, consequently, the error caused by leveling less than 0.06 mgal.

To provide the leveling, the sensor is mounted on a gimbaled frame. Two vertical pendulums mounted on the gimbal frame sense departures from the vertical through comparator circuits. These comparator circuits provide information to stepping motors that drive the gimbals until the pendulums are level. The leveling is accomplished in two modes. When a pendulum is more than 00°32′ of arc from level, the corresponding stepper motor slews faster; at less than 00°32′, the motor slews at a slower rate to avoid overshoot. When the pendulums are within 00°03′ of arc of being level, the slew commands are disabled.

When the instrument has to be inverted in the bias mode, a set of bias pendulums is used that gives signals unless the gimbal frame is similarly leveled in an inverted position.

The TGE can be leveled only if it is initially placed in a position less than 15° from level. In the normal mode, time for leveling is between 0 and 20 sec; in the bias mode, the time is between 90 and 130 sec.

Temperature Control and Monitoring

Because the VSA sensor is extremely sensitive to temperature, it is necessary to control its temperature to within 0.01 K. The VSA and its oscillator-amplifiers are encased in a precision oven that is maintained at a temperature near 322 K to within 0.01 K by the temperature control and monitor circuit. The precision oven, in turn, is encased in an outer oven that protects the inner oven from the external thermal disturbance.

The precision oven temperature circuit has proportional and rate control and uses an electrical heater and a resistance thermometer element for a sensor. The complete temperature sensor is an ac excited bridge, two arms of which are thermistors. The bridge output is demodulated and used to control drivers for the precision heaters. A tap from the demodulator output is converted to digital form and forms a digit of the TGE display. The displayed digit marks the deviations of the precision oven temperature from a preset value. The outer oven thermostat and heater circuit merely react to temperature changes to control the power supplied to a heater.

A thermal blanket provides good thermal insulation for the TGE. A radiator at the top of the instrument provides the primary means of heat expulsion.

The mode of operation of the instrument was such that the radiator was left closed during each EVA. The instrument electronics produced heat, but this heat merely reduced the heating to be done by the ovens. Between EVA periods, the instrument was placed in the shade with the radiator open, and heat was then expelled into space. The temperature monitors are the eighth and ninth digits of the TGE display. The eighth digit gives the thermal condition of the outer oven and the sign for the ninth digit. The ninth digit of the numerical display is a number from 0 to 7 that represents a deviation of the precision oven temperature from a set point of 0.005 K times the digit displayed. Polarity of the deviation is obtained from the value displayed in the eighth digit.

Physical Description of the TGE

The TGE consists of the instrument package, a battery pack assembly, a thermal blanket, and an isoframe assembly. A cutaway view of the TGE is shown in figure 13-3.

Outer Structure.—The outer structure of the TGE is cylindrical with a flat rear surface. A folding handle at the top of the instrument is used for hand carrying and for latching the instrument to the isoframe assembly. Three feet at the base of the instrument enable lunar surface operations. A radiator at the top of the instrument provides the primary means of heat expulsion. The radiator and the display panel are protected from the environment by hinged insulating covers over each.

Inner Structure.—The inner structure of the TGE consists of a two-axis gimbal system, which contains a VSA housed in a thermally protected and evacuated two-stage oven assembly. The oven assembly is enclosed in an electronic frame (E-frame) assembly of similar structural design. The E-frame assembly is pivoted about its axis and supported by a middle

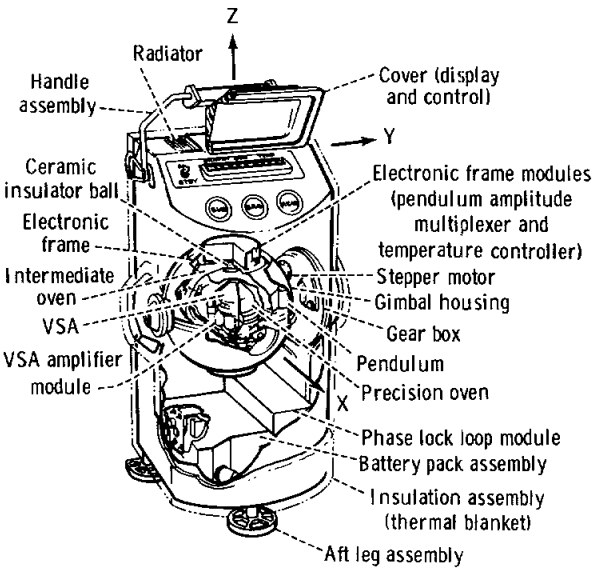

FIGURE 13-3.–Cutaway view of the TGE.

gimbal assembly. The middle gimbal controls the vertical positioning of the inner gimbal over a 30° range. The middle gimbal assembly is attached through bearings to the base housing and can rotate 210°. Stepper motors and a gear train provide the drive and positioning of the gimbal assemblies. The stepper motors react to signals from pendulums that act as level sensors.

Deployment and Operation of Instrument

Gravimeter measurements were made both with the TGE mounted on the lunar roving vehicle (LRV) and with the TGE placed on the surface. During a measurement, the TGE must be placed on a surface such that the vertical axis of the TGE is within 15° of vertical. The TGE must not be disturbed for approximately 3 min after a measurement has been initiated.

A normal measurement (one with the sensor in the normal, vertical position) is initiated by depressing the "GRAV" pushbutton on the TGE (fig. 13-3). The measurement cycle starts with leveling of the instrument. During the leveling cycle, the indicator light flashes off and on. When the instrument comes to a rest within 00°03′ of arc of the vertical, the light stops flashing and remains illuminated until the difference frequency of the strings has been measured. The number of counts of a precision clock (from which the frequency can be obtained) forms the first seven digits of the TGE display. The eighth and ninth digits of the display are thermal monitors, as explained in the section entitled "Temperature Control and Monitoring."

The display stays on for 20 sec. The display can, however, be turned on at any subsequent time by depressing the "READ" pushbutton, and it stays on for 20 sec.

A measurement with the sensor in the inverted position is made by depressing the "BIAS" pushbutton. The bias pendulums are used for leveling, and the indicator light flashes on and off until the sensor is leveled in an inverted position. The counting and display then proceed as for the normal measurement.

To conserve power, a toggle switch is provided to select the "STANDBY" or "ON" mode of operation. In the "STANDBY" mode, power is supplied only to the oven temperature controls and to the VSA oscillator-amplifiers. Cycling the switch from "ON" to "STANDBY" to "ON" will erase any stored data. Depressing the "READ" pushbutton after such a switching provides valid readings only for the eighth digit, which is the temperature monitor for the outer oven and for the battery.

RESULTS

Number of Readings

Of the 26 readings obtained (table 13-I), three (readings 1, 10, and 18) were obtained to learn the thermal state of the instrument before the EVA periods. No gravity values were obtained with these readings.

Reading 8 at the LM site showed that the TGE had been moved during the measurement as indicated by the phase lock loop alarm, which gives zeros in the first three digits of the display in such instances. This reading, therefore, was valueless, and another reading was obtained at the same site.

At the LM site, nine readings were made. Six of these were readings in the normal TGE position (upright) on the lunar surface (readings 3, 9, 11, 17, 19, and 25); one reading was made at the start of each EVA and one at the end of each EVA. Two readings (4 and 26) were made in the inverted position to determine the value of the bias term k_0 at the beginning and end of the measurements. One reading (2) was made on the LRV to compare "on LRV" and "off LRV" measurements.

Besides the readings at the LM site, 11 other

TABLE 13-I.–*Traverse Gravimeter Readings*

Reading	*Location*	*Elapsed time at which measurement initiated, hr:min:sec*	*Display*	$D_n - D_{n\ base}$[a]	$\Delta g = (D_n - D_{n\ base}) \times (-0.03245)$, *mgal*	Δg *after application of empirical correction,*[b] *mgal*	*Elevation, m*	*Comments*
				EVA-1				
1	LM site	–	XXX XXXX OX	–	–	–	–	Thermal monitor reading
2	LM site	01:17:32	670 0031 01	−141	4.6	− 1.4	4510	On LRV
3	LM site	01:40:32	670 0172 01	0	0	0	4510	Off LRV; adopted as base reading D_n base
4	LM site	01:44:29	337 4540 01	–	–	–	–	Off LRV; inverted position
5	ALSEP[c] site	02:15:16	670 0026 01	−146	4.7	− 1.3	4510	On LRV
6	Station 1	05:08:03	670 0129 01	− 43	1.4	− 4.6	4510	On LRV
7	SEP[d] site	05:56:03	670 0101 01	− 71	2.3	− 3.7	4510	On LRV
8	LM site	06:39:44	000 1332 01	–	–	–	–	Off LRV; measurement disturbed and disregarded
9	LM site	06:55:42	670 0215 01	43	− 1.4	− 1.4	4510	Off LRV
				EVA-2				
10	LM site	–	XXX XXXX OX	–	–	–	–	Thermal monitor reading
11	LM site	00:17:46	670 0177 01	5	− 0.2	− 0.2	4510	Off LRV
12	Station 2	02:18:05	670 1552 01	1380	−44.8	−50.8	4625	On LRV
13	Station 2A	03:21:09	670 1235 01	1063	−34.5	−40.5	4605	On LRV
14	Station 3	04:02:40	670 0497 01	325	−10.5	−16.5	4565	On LRV
15	Station 4	04:56:12	670 0125 01	− 47	1.5	− 4.5	4543	On LRV
16	Station 5	06:00:11	670 0314 01	142	− 4.6	−10.6	4525	On LRV
17	LM site	–	670 0235 01	63	− 2.0	− 2.0	4510	Off LRV
				EVA-3				
18	LM site	–	XXX XXXX OX	–	–	–	–	Thermal monitor reading
19	LM site	00:17:20	670 0270 01	98	− 3.2	− 3.2	4510	Off LRV
20	Station 6	01:29:00	670 1098 01	926	−30.0	−36.0	4575	On LRV
21	Station 8	03:20:XX	670 0960 01	788	−25.6	−31.6	4575	On LRV
22	Station 8	03:45:39	670 1173 01	1001	−32.5	−32.5	4575	Off LRV
23	Station 9	04:30:46	670 0378 01	206	− 6.7	−12.7	4515	On LRV
24	Station 9	–	670 0571 01	399	−12.9	−12.9	4515	Off LRV
25	LM site	05:55:58	670 0107 01	− 65	2.1	2.1	4510	Off LRV
26	LM site	06:03:00	337 4171 01	–	–	–	–	Off LRV; inverted position

[a]Difference between the display (first seven digits) at a station D_n and the display at the LM site $D_{n\ base}$ (reading 3).

[b]Empirical correction of − 6.0 mgal applied to all on-LRV values; off-LRV values are unchanged.

[c]Apollo lunar surface experiments package.

[d]Surface electrical properties experiment.

discrete measurements were made at different sites (readings 5, 6, 7, 12, 13, 14, 15, 16, 20, 21, and 23). Two extra measurements (readings 22 and 24) were made at stations 8 and 9 on the lunar surface to compare on-LRV and off-LRV measurements at these sites.

In the preliminary evaluation of gravity in table 13-I, the constants k_2 and k_3 of equation (13-3) are ignored and a value of $k_1 = 0.0001318$ Hz/mgal is assumed. For obtaining the value of gravity Δg at the stations relative to the value at the LM site, it can be shown that, when k_2 and k_3 are ignored, an approximate value is given by

$$\Delta g = \left(D_n - D_{n\ \text{base}}\right) \times (-0.03245) \quad (13\text{-}7)$$

where D_n is the display (first seven digits) at that station and $D_{n\ \text{base}}$ is the display at the LM site. The first off-LRV reading at the LM site (3) was chosen as the $D_{n\ \text{base}}$. The values of Δg thus obtained are given in table 13-I.

Gravimeter Drift

For the flight instrument, it was determined before the mission that the drift during the EVA period ($\approx$ 7 hr) was essentially zero. Therefore, it was decided to adopt a zero drift rate unless the off-LRV values at the LM site showed a consistent drift pattern. The off-LRV values at the LM site are given in table 13-II. Relative to the first reading, the gravity values range from 2.1 to -3.2 mgal. The only positive value, 2.1 mgal, was reading 25. Before reading 25, during the traverse from station 9 to the LM site, the pallet on which the traverse gravimeter was mounted swung open, and, as noted later in the report, the resultant banging of the pallet may have caused instrument problems resulting in an erroneous reading 25. All the remaining values were negative. Nevertheless, a consistent drift pattern was not detected; hence, a zero drift was adopted. The variation in values is attributed to instrument noise, which has an rms value of 1.8 mgal.

TABLE 13-II.–*Off-LRV Δg Values at LM Site Relative to First Value Obtained*
[rms deviation = 1.8 mgal]

Reading	Δg, *mgal*
3	0.0
9	−1.4
11	− .2
17	−2.0
19	−3.2
25	2.1

Comparison of On-LRV and Off-LRV Values

Readings 2 and 3 were both obtained at the LM site. Reading 2 was taken with the gravimeter on the LRV, and reading 3 was taken with the gravimeter on the lunar surface. The difference between the two readings was 4.6 mgal. In an effort to determine whether this difference was random or systematic, on-LRV and off-LRV readings also were taken at stations 8 and 9. As shown in table 13-III, the lunar surface readings are, in all three cases, lower than the LRV values (the free-air difference is negligible) by amounts ranging from 4.6 to 6.9 mgal. There is no explanation for this difference; however, on the basis of three readings, an empirical correction of -6.0 mgal has been made to all on-LRV measurements (table 13-I). Some support for this correction comes also from postmission tests with the engineering and spare flight models. When the handle of the gravimeter was jarred, temporary shifts in the gravimeter measurements occurred that were always in the same direction (although these shifts were <6 mgal). By applying the -6.0-mgal correction to the value at the Apollo lunar surface experiments package (ALSEP) site, this measurement is brought into agreement with the measurement at the LM site. The gravity values at the two sites are expected to be close. However, agreement between the value at the LM site and that at the nearby surface electrical properties (SEP) experiment site deteriorates slightly as a result of this correction.

Earth-Moon Gravity Tie

On the basis of normal reading 3 and inverted reading 4 (table 13-IV), a value of $g = 162\,694.6$ mgal was measured at the LM site at Taurus-Littrow. The constants k_1, k_2, and k_3 used in this determination were obtained during preflight tests. The value of k_0 obtained as a result of readings 3 and 4 was 7.21591 Hz. A predicted value of k_0 based on laboratory test data was 7.2144 Hz. The total shift during the

TABLE 13-III.–*Comparison of Off-LRV and On-LRV Values at LM Site, Station 8, and Station 9*

[rms on-LRV/off-LRV difference without empirical correction, 6.0 mgal; with empirical correction, 1.0 mgal]

Location	*On LRV*		*Off LRV*		*Difference, mgal*	*Difference after application of empirical correction,*[a] *mgal*
	Reading	*Δg, mgal*	*Reading*	*Δg, mgal*		
LM site	2	4.6	3	0.0	4.6	−1.4
Station 8	21	−25.6	22	−32.5	6.9	.9
Station 9	23	− 6.7	24	−12.9	6.2	.2

[a]Empirical correction of − 6.0 mgal applied to on-LRV values.

TABLE 13-IV.–*Determination of* k_0 *and* g *at LM Site from Readings in Normal and Inverted Positions*

Reading	*Position*	*Display*	$\Delta f_n = \frac{192 \times 10^8}{D_n}$, *Hz*	$\Delta f_i = \frac{4.8 \times 10^7}{D_i}$, *Hz*	k_0, *Hz*	g, *mgal*
			EVA-1			
3	Normal	D_n = 670 0172	28.655981	–	7.215910	162 694.6
4	Inverted	D_i = 337 4540	–	14.224161		
			EVA-3			
25	Normal	D_n = 670 0107	28.65626	–	7.215272	162 701.5
26	Inverted	D_i = 337 4171	–	14.225716		

translunar phase was 0.0015 Hz. This corresponds to a bias shift of approximately 11 mgal, which is considered reasonable when compared to typical bias shifts experienced during acceptance and vibration testing.

On the basis of normal reading 25 and inverted reading 26, a second value of g = 162 701.5 mgal was determined after EVA-3. The value for the bias constant k_0 differed by approximately 0.00064 Hz from the initial value, which implies a shift of approximately 5 mgal in the bias value. However, the normal measurement of gravity obtained for reading 25, if the initial value of k_0 is used, differs by only 2 mgal from the initial value. During the traverse from station 9 to the LM site, the pallet on which the traverse gravimeter was mounted apparently swung loose and banged against the LRV. This was the only time during the entire mission that the gravimeter was shocked in this manner. Because deterioration in the performance might have resulted from this shock, less emphasis has been placed on readings 25 and 26 and the initial determination of 162 694.6 mgal has been adopted. An uncertainty of ± 5 mgal is ascribed to this measurement.

DISCUSSION

Computation of Bouguer Anomalies

For a preliminary interpretation of the gravity measurement, two-dimensionality is assumed. The problem then essentially is reduced to the determination of the substructure of the linear Taurus-Littrow valley with linear massifs on either side. The stations at which the gravity measurements were made are shown in figure 13-4; the values at these stations were projected to a roughly southwest-to-northeast cross section. The value at station 6 could not be appropriately projected to this cross section and has been ignored in the present discussion. The great structural relief of the area makes three-dimensional calculations necessary. Such calculations will be described in

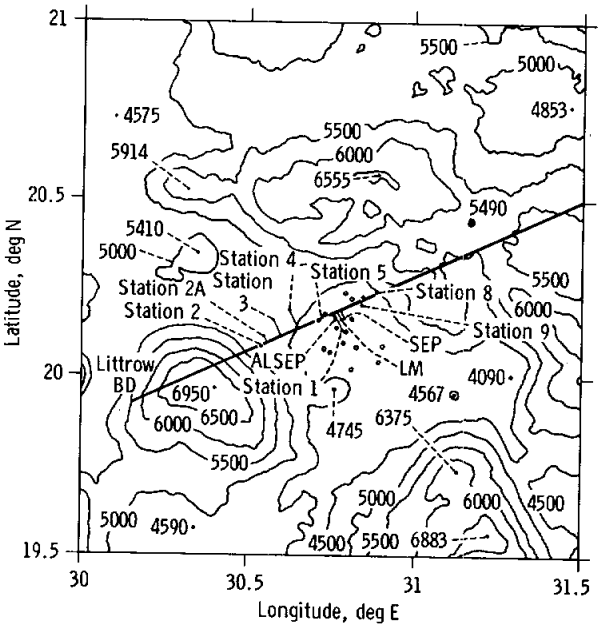

FIGURE 13-4.–Contour map of Taurus-Littrow landing site, showing the stations at which gravity measurements were made. The straight line starting near Littrow BD Crater (lower left) and trending northeast through the landing site is the cutting plane for the cross section to which the gravity measurements were projected. (Based on operational topographic map prepared by U.S. Army Topographic Command, October 1972. Contour interval, 500 m.)

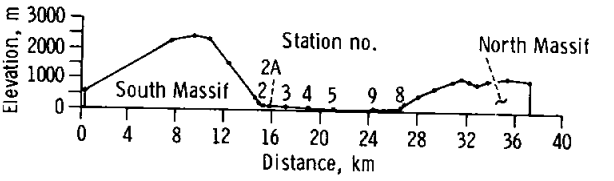

FIGURE 13-5.–Topographic profile showing locations of projected stations. Station 1 and the ALSEP and SEP sites have been omitted because their elevations are the same as that of the LM site. The elevation datum (abscissa) is the elevation of the LM site.

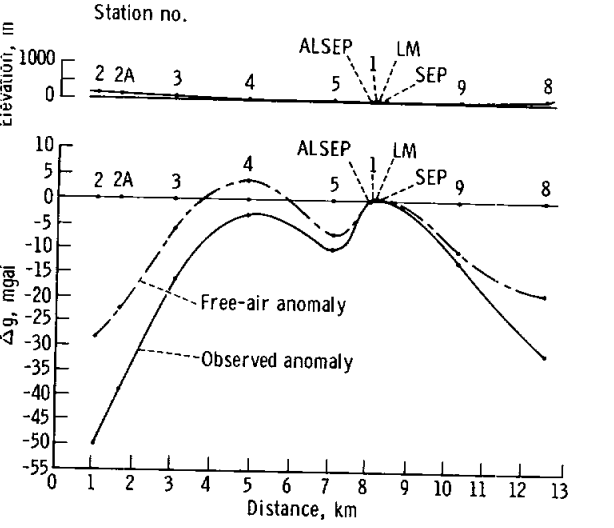

FIGURE 13-6.–Observed anomaly and free-air anomaly profiles across the Taurus-Littrow valley.

a later report. The topographic profile with the locations of the projected stations is shown in figure 13-5.

The observed anomaly Δg, as obtained in table 13-I, is plotted as a function of distance in figure 13-6. The observed anomaly is approximately 50 mgal lower at station 2, closest to the South Massif, and approximately 30 mgal lower at station 8, closest to the North Massif, relative to the value of gravity at the LM site. The observed anomaly curve therefore shows a pronounced dip toward the massifs on either side.

The free-air correction is applied by using the correction previously given, $2g_m/r$. The free-air anomaly thus obtained (also plotted in fig. 13-6) dips to approximately -30 mgal near the South Massif and to -20 mgal near the North Massif relative to the value at the LM site.

The Bouguer correction is applied next. In making the free-air correction, as well as the Bouguer correction, an elevation datum must be chosen (fig. 13-1). The elevation datum chosen was the elevation of the LM site (fig. 13-5), which was the lowest elevation on the profile.

The Bouguer correction is, in effect, made in three parts to show the effect of (1) the valley floor (i.e., material lying between the elevation of the stations and the elevation datum; shown with a density of ρ_2 in fig. 13-1), (2) the North Massif, and (3) the South Massif. The three Bouguer correction curves and the total Bouguer correction are shown in figure 13-7. Note that the effect of the valley floor tends to cancel the effect of the massifs; hence, the total Bouguer effect is quite small (< 5 mgal). The Bouguer correction was calculated using a density of 2.0 g/cm^3 ($\rho_1 = \rho_2 = 2.0$ g/cm^3). This value is lower than the values for breccia densities shown in figure 13-8(a). However, if an average density of 2.5 g/cm^3 were used instead of 2.0 g/cm^3, the difference in the

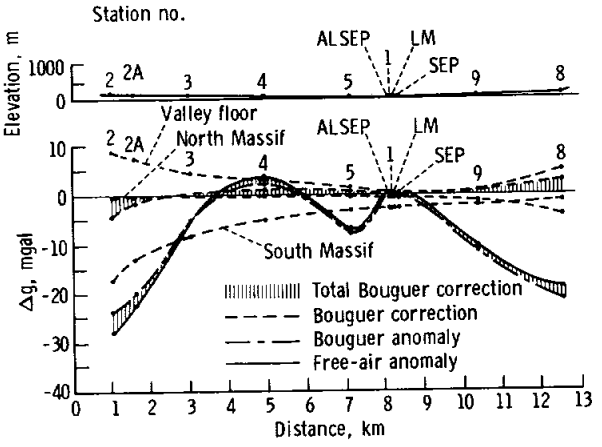

FIGURE 13-7.–Application of the Bouguer correction to determine the Bouguer anomaly profile across the Taurus-Littrow valley, showing the effect of the valley floor, of the North Massif, and of the South Massif and the total Bouguer correction. The free-air anomaly curve (fig. 13-6) is included for comparison with the Bouguer anomaly curve.

computed total correction would, in all cases, be less than 1 mgal. That difference can be ignored for the present discussion.

The resultant Bouguer anomaly curve, included in figure 13-9, shows minimums of near – 25 mgal at the stations closest to the massifs. The variation in the central part of the valley floor is within 10 mgal of the value at the LM site. This curve has to be interpreted in terms of the substructure of the valley. To do so, what is known about the densities of the lunar rocks must be considered first.

Densities of Lunar Rocks

No particular effort has yet been made to measure the bulk densities of the returned lunar rock samples. However, a few measured density values have been reported in the literature (refs. 13-3 to 13-21).[1] Most of these values were obtained in the course of measuring other physical properties of the lunar rocks (e.g., seismic velocity, heat conductivity, etc.). These published values are plotted in the histograms in figures 13-8(a) (lunar breccias) and 13-8(b) (lunar basalts).

The method used to obtain the density values was not always indicated in the sources but, when given, was one of the following.

1. The volumes of aluminum foil models of the whole rocks were measured, and the bulk densities were computed using the weights of the rocks. Because the aluminum foil models were not made to great accuracy, these density values can have 10 percent or even greater errors.

2. The volumes of small, precisely shaped samples of the rocks were computed by measuring their linear dimensions. The small samples are generally parallelepipeds, 1 by 1 by 2 cm. The densities were then computed using the measured weights of the small samples.

3. The densities of some small samples were measured directly using Archimedes' principle.

The density values tended to group on the basis of the method used to compute the density: the first method giving low values, the third method giving high values, and the second method giving values in the middle. This result is reasonable because the samples were generally vuggy, vesicular, porous, or highly fractured. Thus, the first method includes the effects of the largest vugs and vesicles and the third method includes only the effect of the unconnected pores and cracks; the second method will generally eliminate the effect of large vesicles and vugs but not that of small cracks and pores that cannot be avoided in cutting the small samples. Thus, an intrinsic density of approximately 3.4 g/cm^3 for the lunar basalts is indicated in figure 13-8(b).

Porosities have been measured for a few samples by point counts on thin sections or cut surfaces. A plot of density as a function of porosity and the intrinsic densities calculated from the porosities is given in figure 13-10. The intrinsic densities range from 3.25 to 3.49 g/cm^3 for the three basalts and from 2.99 to 3.14 g/cm^3 for the five breccias.

Figures 13-8(b) and 13-10 indicate that the bulk densities of mare basalt samples are determined by their porosity and that the samples have an intrinsic density of approximately 3.4 g/cm^3. Thus, a thick, mare lava flow with a thin, vesicular top would have a bulk density somewhat less than 3.4 g/cm^3. The data on the breccias are not as conclusive, but there is no evidence that the highly fractured rocks and breccias forming the highlands are more dense, on the average, than the average of the breccia samples thus far reported. Therefore, the density contrast between a

[1] Also N. Warren, private communication, 1972, and G. D. O'Kelley, personal communication, 1973.

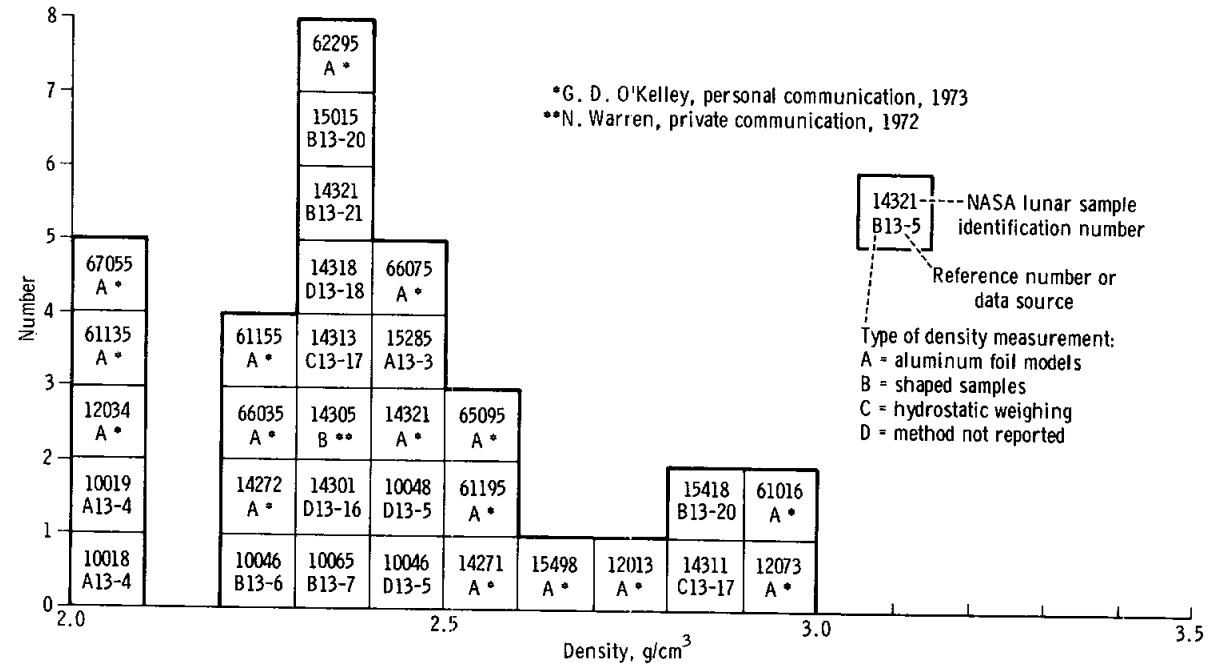

(a)

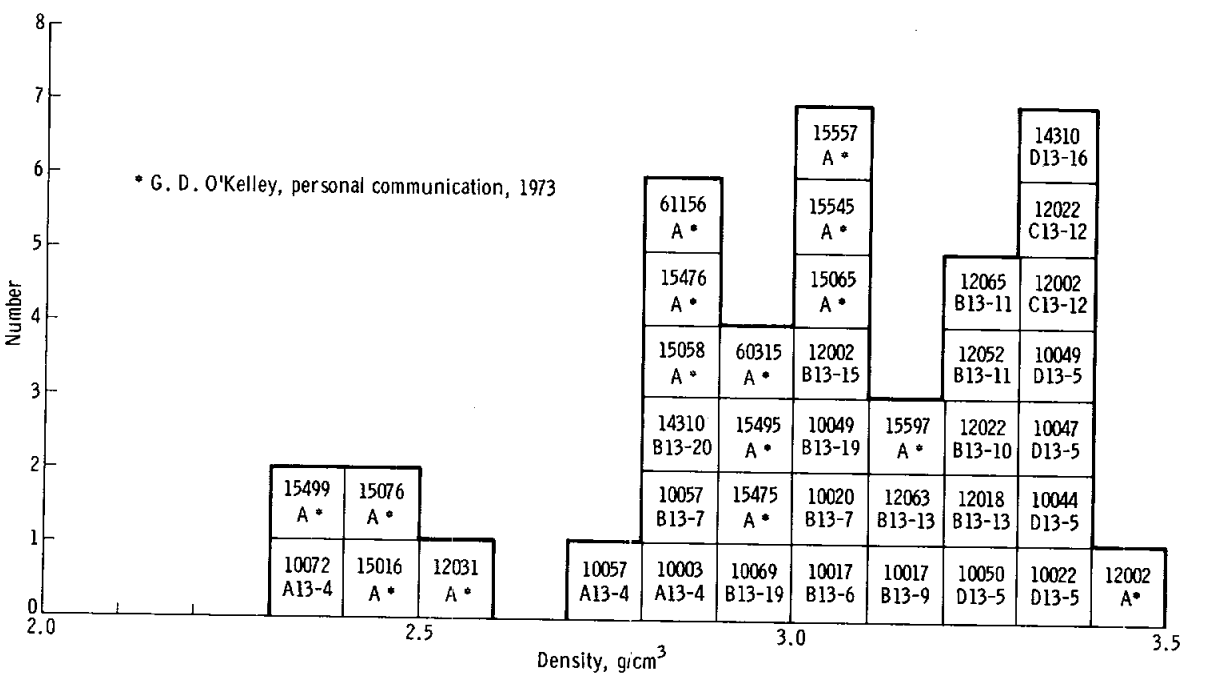

(b)

FIGURE 13-8.–Measured density values for lunar samples. (a) Breccia. (b) Basalt.

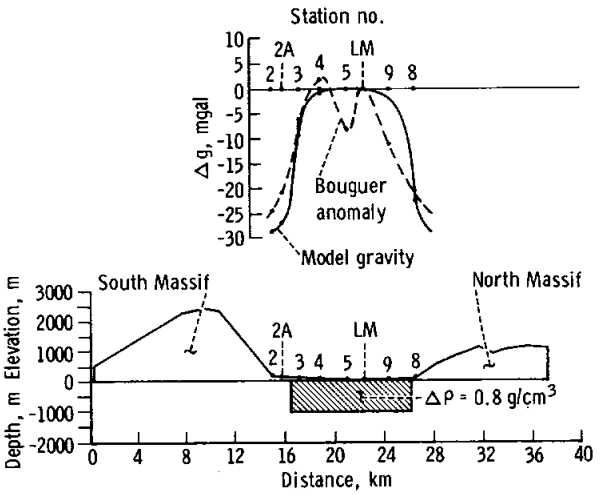

FIGURE 13-9.–Assumed model for subvalley densities to explain gravity anomalies, including the Bouguer anomaly curve. On the ordinate for the topographic profile, the elevation and depth are referenced to the elevation datum (0 m), which is the elevation of the LM site. The shaded rectangle represents a postulated block of basaltic material underlying the valley floor, where $\Delta\rho$ is the positive density contrast with respect to brecciated highland material on either side.

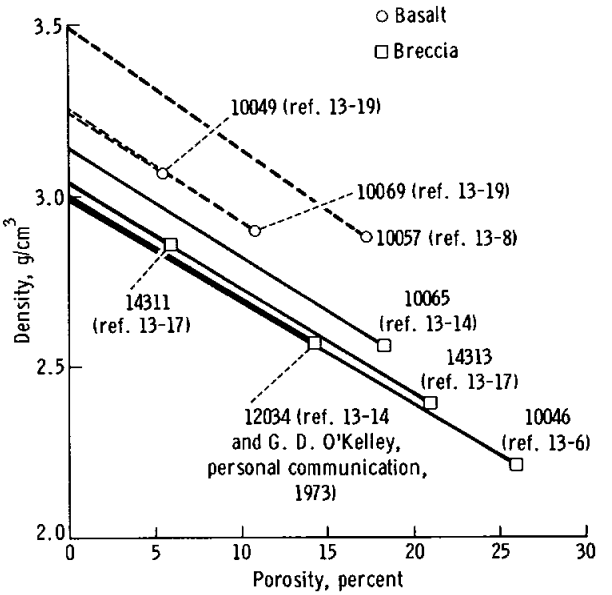

FIGURE 13-10.–Dependence of density on porosity for breccia and basalt lunar samples.

thick, mare basalt formation and highland breccia material should be at least $3.2 - 2.8 = 0.4$ g/cm^3 and may be as much as $3.3 - 2.3 = 1.0$ g/cm^3.

Structural Model

From the results of the last section, a very simple model has been used to explain the gravity results. Assuming that the subvalley floor material consists of basalt flows that have a positive density contrast of 0.8 g/cm^3 with respect to brecciated highland material on either side, a thickness of 1 km is obtained for the block of basaltic material (fig. 13-9). The large Bouguer gradients at the valley edges indicate steep sides for the postulated block of basaltic material. The sides are not at the edges of the valley but lie approximately 1 km inside the edges of the valley.

These are very preliminary conclusions based on the work performed to date. More elaborate models have not been presented because we expect that the three-dimensional terrain and Bouguer corrections will change the final Bouguer anomalies by 30 to 40 percent. These three-dimensional calculations will be based on the newer topographic maps currently being compiled. Changes are expected in the total Bouguer anomaly amplitude (from edge of valley to center of valley) as well as in the slope of the Bouguer anomaly curve near the edges. In this connection, the values obtained at stations 2A and 6 will be especially useful in refining the nature and position of the margin of the inferred high-density body underlying the valley floor.

SUMMARY AND CONCLUSIONS

The successful performance of the TGE indicated that the value of gravity at the Taurus-Littrow landing site is 162 694.6 ± 5 mgal. The Bouguer anomaly, analyzed with a two-dimensional approximation, shows values approximately 25 mgal lower at the edges of the valley than at the LM site. The Bouguer anomaly curve is interpreted in terms of a 1-km-thick block of basaltic material lying below the valley floor with a positive density contrast of 0.8 g/cm^3 with respect to the material on either side.

REFERENCES

13-1. Talwani, Manik; Worzel, J. Lamar; and Landisman, Mark: Rapid Gravity Computations for Two-Dimensional Bodies with Application to the Mendocino Submarine Fracture Zone. J. Geophys. Res., vol. 64, no. 1, Jan. 1959, pp. 49-59.

13-2. Jung, K.: Schwerkraftverfahren in der Angewandten Geophysik. Akademische Verlags Gesellschaft, Geest and Portig K. (–G.), Leipzig, Germany, 1961.

13-3. O'Kelley, G. Davis; Eldridge, James S.; Schonfeld, E.; and Northcutt, K. J.: Concentrations of Primordial Radioelements and Cosmogenic Radionuclides in Apollo 15 Samples by Nondestructive Gamma-Ray Spectrometry. Lunar Science-III (Rev. abs. of the Third Lunar Science Conference (Houston, Tex.), Jan. 10-13, 1972), pp. 587-589.

13-4. O'Kelley, G. D.; Eldridge, J. S.; Schonfeld, E.; and Bell, P. R.: Primordial Radionuclide Abundances, Solar Proton and Cosmic Ray Effects and Ages of Apollo 11 Lunar Samples by Nondestructive Gamma-Ray Spectrometry. Proceedings of the Apollo 11 Lunar Science Conference, vol. 2, Pergamon Press (New York), 1970, pp. 1407-1423.

13-5. Schmitt, H. H.; Lofgren, G.; Swann, G. A.; and Simmons, G.: The Apollo 11 Samples: Introduction. Proceedings of the Apollo 11 Lunar Science Conference, vol. 1, Pergamon Press (New York), 1970, pp. 1-54.

13-6. Anderson, O. L.; Scholz, C.; Soga, N.; Warren, N.; and Schreiber, E.: Elastic Properties of a Micro-Breccia, Igneous Rock and Lunar Fines from Apollo 11 Mission. Proceedings of the Apollo 11 Lunar Science Conference, vol. 3, Pergamon Press (New York), 1970, pp. 1959-1973.

13-7. Horai, K.; Simmons, G.; Kanamori, H.; and Wones, D.: Thermal Diffusivity, Conductivity and Thermal Inertia of Apollo 11 Lunar Material. Proceedings of the Apollo 11 Lunar Science Conference, vol. 3, Pergamon Press (New York), 1970, pp. 2243-2249.

13-8. Kanamori, H.; Nur, A.; Chung, D. H.; and Simmons, G.: Elastic Wave Velocities of Lunar Samples at High Pressures and Their Geophysical Implications. Proceedings of the Apollo 11 Lunar Science Conference, vol. 3, Pergamon Press (New York), 1970, pp. 2289-2293.

13-9. Stephens, D. R.; and Lilley, E. M.: Loading-Unloading Pressure-Volume Curves to 40 kbar for Lunar-Crystalline Rock, Micro-Breccia and Fines. Proceedings of the Apollo 11 Lunar Science Conference, vol. 3, Pergamon Press (New York), 1970, pp. 2427-2434.

13-10. Stephens, D. R.; and Lilley, E. M.: Pressure-Volume Properties of Two Apollo 12 Basalts. Proceedings of the Second Lunar Science Conference, vol. 3, MIT Press (Cambridge, Mass.), 1971, pp. 2165-2172.

13-11. Kanamori, H.; Mizutani, H.; and Hamano, Y.: Elastic Wave Velocities of Apollo 12 Rocks at High Pressures. Proceedings of the Second Lunar Science Conference, vol. 3, MIT Press (Cambridge, Mass.), 1971, pp. 2323-2326.

13-12. Wang. H.; Todd, T.; Weidner, D.; and Simmons, G.: Elastic Properties of Apollo 12 Rocks. Proceedings of the Second Lunar Science Conference, vol. 3, MIT Press (Cambridge, Mass.), 1971, pp. 2327-2336.

13-13. Warren, N.; Schreiber, E.; Scholz, C.; Morrison, J. A.; et al.: Elastic and Thermal Properties of Apollo 11 and Apollo 12 Rocks. Proceedings of the Second Lunar Science Conference, vol. 3, MIT Press (Cambridge, Mass.), 1971, pp. 2345-2360.

13-14. Chao, E. C. T.; Boreman, J. A.; and Desborough, G. A.: The Petrology of Unshocked and Shocked Apollo 11 and Apollo 12 Micro-Breccias. Proceedings of the Second Lunar Science Conference, vol. 1, MIT Press (Cambridge, Mass.), 1971, pp. 797-816.

13-15. Katsube, T. J.; and Collett, L. S.: Electrical Properties of Apollo 11 and Apollo 12 Lunar Samples. Proceedings of the Second Lunar Science Conference, vol. 3, MIT Press (Cambridge, Mass.), 1971, pp. 2367-2379.

13-16. Chung, D. H.; and Westphal, W. B.: Dielectric Properties of Apollo 14 Lunar Samples. Lunar Science–III (Rev. abs. of the Third Lunar Science Conference (Houston, Tex.), Jan. 10-13, 1972), pp. 139-140.

13-17. Mizutani, H.; Fujii, N.; Hamano, Y.; Osako, M.; and Kanamori, H.: Elastic Wave Velocities and Thermal Diffusivities of Apollo 14 Rocks. Lunar Science–III (Rev. abs. of the Third Lunar Science Conference (Houston, Tex.), Jan. 10-13, 1972), pp. 547-549.

13-18. Chung, Dae H.: Laboratory Studies on Seismic and Electrical Properties of the Moon. The Moon, vol. 4, nos. 3/4, June/July 1972, pp. 356-372.

13-19. Horai, Ki-iti; and Fujii, Naoyuki: Thermophysical Properties of Lunar Material Returned by Apollo Missions. The Moon, vol. 4, nos. 3/4, June/July 1972, pp. 447-475.

13-20. Todd, Terrence; Wang, Herbert; Baldridge, W. Scott; and Simmons, Gene: Elastic Properties of Apollo 14 and 15 Rocks. Proceedings of the Third Lunar Science Conference, vol. 3, MIT Press (Cambridge, Mass.), 1972, pp. 2577-2586.

13-21. Chung, D. H.; Westphal, W. B.; and Olhoeft, G. R.: Dielectric Properties of Apollo 14 Lunar Samples. Proceedings of the Third Lunar Science Conference, vol. 3, MIT Press (Cambridge, Mass.), 1972, pp. 3161-3172.